Iranian Journal of Electrical and Electronic Engineering 01 (2020) 26–38
Special Issue on Electrical Machines and Drives

IUST Iran University of Science and Technology

Iranian Journal of Electrical and Electronic Engineering

Journal Homepage: ijeee.iust.ac.ir

Research Paper

A New Subdomain Method for Performances Computation in Interior Permanent-Magnet (IPM) Machines

A. Jabbari*(C.A.) and F. Dubas**

Abstract: In this research work, an improved two-dimensional semi-analytical subdomain based method for performance computation in IPM machine considering infinite-/finite-magnetic material permeability in pseudo-Cartesian coordinates by using hyperbolic functions has been presented. In the developed technique, all subdomains are divided into periodic or non-periodic regions with homogeneous or non-homogeneous boundary conditions (BCs), respectively. Taking into account the appropriate interfaces conditions in the presented coordinates system, the machine performances including magnetic flux density, cogging/electromagnetic torque, back-EMF, and self-/mutual induction have been calculated for three distinct values of soft-magnetic material relative permeability (viz, 200, 800 and ∞). The semi-analytical results are compared and confirmed by the FEA results.

Keywords: IPM Machine, Analytical Model, Soft-Magnetic Material Relative Permeability, Pseudo-Cartesian Coordinates, Subdomain-Based Technique.

1 Introduction

INTERIOR permanent magnet (IPM) machines are a good candidate to replace surface-mounted PM machines in high-speed applications. Accurate analytical computation of the electromagnetic characteristics of the IPM machines is important, especially in design and optimization stage. Due to property variation of iron parts in different directions, intrinsic UMF [1-5] and therefore, a local/global saturation of these parts occurs [6-17]. In general, numerical methods are attractive due to their high precision for estimating the electromagnetic performances in IPM machines [18]. However, the main drawback of these methods is their long computing time [19]. The magnetic vector potential calculation in electrical machines can be found in [4-12] and [15-39].

Subdomain based techniques are well known as exact analytical methods, with a very well accord compared to FEA. However, some definite physical and geometrical presumptions are considered in these techniques. The most important presumption in subdomain approaches is that soft-magnetic materials permeability is considered infinite [27-30]. Some works have covered the distinct values of soft-magnetic material relative permeability and the saturation effect in subdomain based approaches. In non-periodic regions due to the property variation of iron parts in different directions, the boundary conditions are considered non-homogeneous. But then, the harmonic modeling approach is used in a few kinds of research to consider the soft-magnetic material permeability [6-11].

To the best of the authors' knowledge, some analytical models are available to include the distinct iron parts relative permeability and the saturation effect in semi-analytical approaches using the subdomain technique in [6-17]. A subdomain based analytical model was presented in Cartesian coordinates [13] and polar coordinates [14] by resolution of Laplace's and Poisson's equations in an air-/iron-cored coil. The iron-pieces relative permeability is considered during the electromagnetic computation of IPM machines [12], wherein; r-edge integrated circuits are realized using Taylor series expansion. Roubache *et al.* [15] introduced a subdomain method for the prediction of the electromagnetic performance in electrical machines

Iranian Journal of Electrical and Electronic Engineering, 2020.
Paper first received 12 May 2019, revised 19 August 2019, and accepted 25 August 2019.
* The author is with the Mechanical Engineering Department, Arak University, Arak, Iran.
E-mail: a-jabbari@araku.ac.ir.
** The author is with the Département ENERGIE, FEMTO-ST, CNRS, Univ. Bourgogne Franche-Comté, F90000 Belfort, France.
E-mail: fdubas@gmail.com.
Corresponding Author: A. Jabbari.

with radial magnetization orientation taking into account the distinct iron parts relative permeability.

Therefore, the main contribution of the proposed work is to improve the semi-analytical model presented in [14] for prediction of electromagnetic performances in IPM machines considering the finite soft-magnetic parts relative permeability at no-load and on-load conditions. In the presented method, Maxwell's equations have been solved in non-periodic regions in pseudo-Cartesian coordinates system taking into account the non-homogeneous boundary conditions. In order to calculate the integration constants, the interface conditions are applied in different directions. All the results of the proposed method are then compared in amplitudes and waveforms to those found by the 2-D FEA.

2 Problem Definition and Assumption

A schematic representation of the studied machine with the following regions is shown in Fig. 1.

- Subdomain I: the rotor shaft;
- Subdomain II: the rotor yoke;
- Subdomain III: the rotor teeth,
- Subdomain IV: the rotor slot;
- Subdomain l: the PMs;
- Subdomain k: the rotor teeth;
- Subdomain V: the rotor teeth;
- Subdomain VI: the air-gap;
- Subdomain VI: the stator teeth;
- Subdomain VII: the stator slot (on the left);
- Subdomain VIII: the stator slot (on the right);
- and Subdomain X: the stator yoke.

The general partial differential equation in an isotopic subdomain can be expressed by

$$\nabla^2 A_z = 0 \text{ in Subdomains I, II, III, k, V, VI, IX, X} \quad (1)$$

$$\nabla^2 A_z = -\mu_0 \nabla \times \boldsymbol{M} \text{ in Subdomain l} \quad (2)$$

$$\nabla^2 A_z = -\mu_0 J \text{ in Subdomains VII and VIII} \quad (3)$$

where μ_0 is the vacuum permeability, $\boldsymbol{M}$ is the PM magnetization and J_z is the current density.

The field vectors $\boldsymbol{B}$={B_t; B_θ; 0} and $\boldsymbol{H}$={H_t; H_θ; 0} in all subdomains are paired by the magnetic material equation:

$$\boldsymbol{B} = \mu_0 \boldsymbol{H} \text{ in Subdomains I, IV, and VI} \quad (4)$$

$$\boldsymbol{B} = \mu_0 \mu_{rm} H + \mu_0 \boldsymbol{M} \text{ in Subdomain l} \quad (5)$$

$$\boldsymbol{B} = \mu_0 \mu_{rc} \boldsymbol{H} \text{ in Subdomains II, III, k, V, IX, and X} \quad (6)$$

where μ_{rm} and μ_{rc} are the relative recoil permeability of PMs and iron pieces, respectively. Using $\boldsymbol{B} = \nabla \times \boldsymbol{A}$ the components of $\boldsymbol{B}$ can be concluded by

$$B_t = \frac{e^t}{R_i}\frac{\partial A_z}{\partial \theta} \quad (7)$$

and

$$B_\theta = \frac{e^t}{R_i}\frac{\partial A_z}{\partial t} \quad (8)$$

3 Resolution of Maxwell's Equations

In this section, firstly, we categorize each subdomain as the periodicity or non-periodicity Subdomain. The resolution of PDE equation in each subdomain has then been performed considering the appropriate BC and IC in order to determine the integration constants.

3.1 Periodic Subdomains

Periodic Subdomains include the stator yoke, the air-gap, the rotor yoke, and the rotor shaft subdomains, with a period interval of 2π. In the periodic Subdomains, the following Laplace's equation has to be solved:

$$\frac{\partial^2 A_\Omega}{\partial t^2} + \frac{\partial^2 A_\Omega}{\partial \theta^2} = 0 \quad (9)$$

where Ω is X, VI, II, and I for the Subdomains of the stator yoke, air-gap, rotor yoke and rotor shaft, respectively.

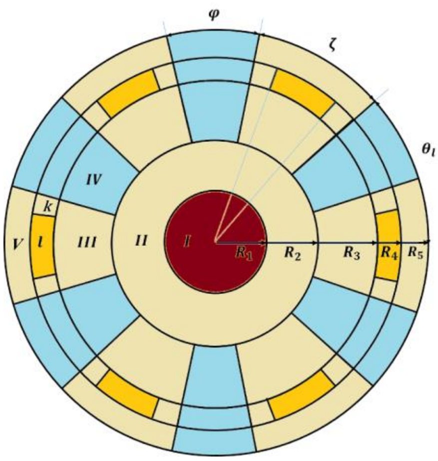

(a)

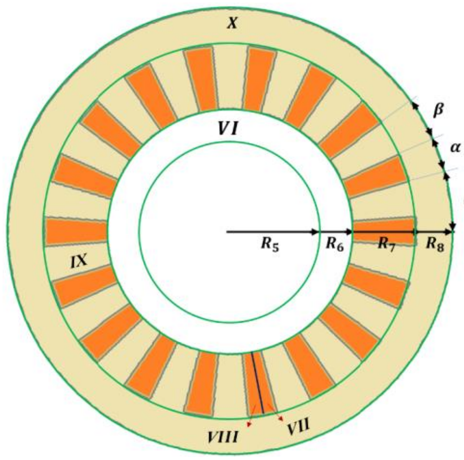

(b)

Fig. 1 The investigated model: a) the rotor subdomains, and b) the stator subdomains.

Considering the $\theta \in [0, 2\pi]$ for the machine, (9) becomes

$$
\begin{aligned}
&A_{z\Omega}(t.\theta) = a_0^{\Omega} + b_0^{\Omega} t \\
&+\sum_{n=1}^{\infty}\left(a_n^{\Omega}\frac{F\left(n\left(t-t_j\right)\right)}{Sh\left(n\left(t_i-t_j\right)\right)} + b_n^{\Omega}\frac{F\left(n\left(t-t_i\right)\right)}{Sh\left(n\left(t_j-t_i\right)\right)}\right)\cos\left(n\theta\right) \\
&+\sum_{n=1}^{\infty}\left(c_n^{\Omega}\frac{F\left(n\left(t-t_j\right)\right)}{Sh\left(n\left(t_i-t_j\right)\right)} + d_n^{\Omega}\frac{F\left(n\left(t-t_i\right)\right)}{Sh\left(n\left(t_j-t_i\right)\right)}\right)\sin\left(n\theta\right) \quad (10)
\end{aligned}
$$

where n is a positive integer, $F = Sh$, $t\in[t_i=t_1,\ t_j=t_2]$ and $b_n^{\Omega}=d_n^{\Omega}=0$ for rotor shaft (Ω=I), $F=Sh$ and $t\in[t_i=t_3,\ t_j=t_4]$, for rotor yoke (Ω=II), $F=Sh$, $t\in[t_i=t_{15},\ t_j=t_{16}]$ and $b_n^{\Omega}=d_n^{\Omega}=0$ for stator yoke (Ω=X), $F=Ch$ and $t\in[t_i=t_{11},\ t_j=t_{12}]$ for air-gap (Ω=VI).

3.2 Non-Periodic Subdomains

The stator teeth, the stator slot-opening, the rotor slot, the rotor teeth, the stator slot-right side, the stator slot-left side, and the PM Subdomains are non-periodic Subdomains. Taking into account the Poisson's equation for the stator slot and the PM Subdomains, Laplace's equation is considered for the other non-periodic subdomains.

3.2.1 General solution of Laplace's Equation

Using the principle of superposition [14], the resolution of Laplace's equation in non-periodic Subdomains is given by:

$$
\begin{aligned}
&for\begin{cases} \nu_{h.\Omega(g)} = h\pi/\Theta \\ \nu_{k.\Omega(g)} = k\pi/t_j \end{cases} \\
&A_{z\Omega(g)}(t.\theta) = a_0^{\Omega(g)} + b_0^{\Omega(g)} t \\
&+\sum_{h=1}^{\infty}\left(\frac{a_h^{\Omega(g)}}{\nu_{h.\Omega(g)}}\frac{F\left(\nu_{h.\Omega(g)}\left(t-t_j\right)\right)}{Sh\left(\nu_{h.\Omega(g)}\left(t_i-t_j\right)\right)} \right. \\
&\qquad \left. + \frac{b_h^{\Omega(g)}}{\nu_{h.\Omega(g)}}\frac{F\left(\nu_{h.\Omega(g)}\left(t-t_i\right)\right)}{Sh\left(\nu_{h.\Omega(g)}\left(t_j-t_i\right)\right)}\right)\cos\left(\nu_{h.\Omega(g)}\left(\theta-\theta_1\right)\right) \\
&+\sum_{k=1}^{\infty}\left(\frac{a_k^{\Omega(g)}}{\nu_{k.\Omega(g)}}\frac{Sh\left(\nu_{k.\Omega(g)}\left(\theta-\theta_1\right)\right)}{Sh\left(\nu_{k.\Omega(g)}\Theta\right)} \right. \\
&\qquad \left. + \frac{b_k^{\Omega(g)}}{\nu_{k.\Omega(g)}}\frac{Sh\left(\nu_{k.\Omega(g)}\left(\theta-\theta_2\right)\right)}{Sh\left(\nu_{k.\Omega(g)}\Theta\right)}\right)\sin\left(\nu_{k.\Omega(g)} t\right) \quad (11)
\end{aligned}
$$

where $t\in[t_{13},\ t_{14}]$, $\Theta=\beta$, $\theta\in[\theta_1,\ \theta_2]=[\theta_i+\alpha\theta\text{i}+\alpha+\beta]$, $\Omega(g)$=IX(m) and $F=Ch$ for m-th stator teeth, $t\in[t_9,\ t_{10}]$, $\Theta=\zeta$, $\theta\in[\theta_l,\ \theta_l+\zeta]$, $a_k^{\Omega(g)}=b_k^{\Omega(g)}=0$, $F=Sh$ and $\Omega(g)=V(k)$ for k-th rotor teeth, $t\in[t_5,\ t_{10}]$, $\Theta=\varphi$, $\theta\in[\theta_l+\zeta,\ \theta_l+\zeta+\varphi]$, $F=Ch$ and $\Omega(g)$=IV(j) for j-th rotor slot.

3.2.2 Resolution of Poisson's Equation

A. Stator Slot

In the Subdomain VII(m) and the Subdomain VIII(m), we have to solve (12), that is the Poisson's equations,

$$
\frac{\partial^2 A_{\Omega}}{\partial t^2} + \frac{\partial^2 A_{\Omega}}{\partial \theta^2} = -\mu_0 R_6^{\,2} e^{-2t} J_{zi} \qquad (12)
$$

where J_{zi} is the current density.

Using the principle of superposition [14] and the separation of variables method, (12) becomes

$$
\begin{aligned}
&A_{z\Omega(g)}(t.\theta) = a_0^{\Omega(g)} + b_0^{\Omega(g)} t - \frac{1}{4}\mu_0 J_{z\Omega(g)} e^{-2t} \\
&+\sum_{h=1}^{\infty}\frac{a_h^{\Omega(g)}}{\nu_{h.\Omega(g)}}\frac{Ch\left(\left(2h\pi/\alpha\right)\left(t-t_{14}\right)\right)}{Sh\left(\left(2h\pi/\alpha\right)\left(t_{13}-t_{14}\right)\right)}\cos\left(\left(2h\pi/\alpha\right)\left(\theta-\theta_1\right)\right) \\
&+\sum_{k=1}^{\infty}\left(\frac{a_k^{\Omega(g)} t_{14}}{k\pi}\frac{Sh\left(\left(k\pi/t_{14}\right)\left(\theta-\theta_1\right)\right)}{Sh\left(k\pi\alpha/2t_{14}\right)} \right. \\
&\qquad \left. + \frac{b_k^{\Omega(g)} t_{14}}{k\pi}\frac{Sh\left(\left(k\pi/t_{14}\right)\left(\theta-\theta_2\right)\right)}{Sh\left(k\pi\alpha/2t_{14}\right)}\right)\sin\left(\left(k\pi/t_{14}\right)t\right) \quad (13)
\end{aligned}
$$

where $\theta\in[\theta_i,\ \theta_i+\alpha/2]$ and $\Omega(g)$=VII(m) for m-th stator slot-right side and $\theta\in[\theta_i+\alpha/2,\ \theta_i+\alpha]$ and $\Omega(g)$=VIII(m) for m-th stator slot-left side.

B. Permanent Magnet Subdomain (Subdomain *l*)

In the Subdomain $l(i)$, the Poisson's equation can be rewritten as,

$$
\frac{\partial^2 A_{\Omega(g)}}{\partial t^2} + \frac{\partial^2 A_{\Omega(g)}}{\partial \theta^2} = \mu_0 R_3 e^{-t}\frac{\partial M_r}{\partial \theta} \qquad (14)
$$

where M_r is radial components of magnetization.

Using the separation of variables method, resolution of (14) for j-th PM Subdomain led to

$$
\begin{aligned}
&A_{z\Omega(g)}(t.\theta) = a_0^{\Omega(g)} + b_0^{\Omega(g)} t - R_3 e^{-t}\left(-1\right)^i B_r\left(\theta-\theta_1\right) \\
&+\sum_{h=1}^{\infty}\left(\frac{a_h^{\Omega(g)}\zeta}{h\pi}\frac{Ch\left(\left(h\pi/\zeta\right)\left(t-t_8\right)\right)}{Sh\left(\left(h\pi/\zeta\right)\left(t_7-t_8\right)\right)} \right. \\
&\qquad + \frac{b_h^{\Omega(g)}\zeta}{h\pi}\frac{Ch\left(\left(h\pi/\zeta\right)\left(t-t_7\right)\right)}{Sh\left(\left(h\pi/\zeta\right)\left(t_8-t_7\right)\right)} \\
&\qquad \left. + X_h^I(t)\cos\left(\left(h\pi/\zeta\right)\varphi_i\right)\right)\cos\left(\left(h\pi/\zeta\right)\left(\theta-\theta_1\right)\right) \\
&+\sum_{k=1}^{\infty}\left(\frac{a_k^{\Omega(g)} t_8}{k\pi}\frac{Sh\left(\left(k\pi/t_8\right)\left(\theta-\theta_1\right)\right)}{Sh\left(\left(k\pi/t_8\right)\zeta\right)} \right. \\
&\qquad \left. + \frac{b_k^{\Omega(g)} t_8}{k\pi}\frac{Sh\left(\left(k\pi/t_8\right)\left(\theta-\theta_2\right)\right)}{Sh\left(\left(k\pi/t_8\right)\zeta\right)}\right)\sin\left(\left(k\pi/t_8\right)t\right) \quad (15)
\end{aligned}
$$

where k is a positive integer and the coefficients $a_h^{\Omega(g)}$, $b_h^{V\Omega(g)}$, $a_k^{\Omega(g)}$, and $b_k^{\Omega(g)}$ are determined based on the continuity and ICs.

4 Results and Evaluation

The two-dimensional semi-analytical model for IPM machine considering the distinct iron parts relative permeability is applied to predict the magnetic vector potential components, the back electromotive force, the cogging torque, the electromagnetic torque and the self-/mutual inductances in three distinct machines. The topology of each studied machine is shown in Fig. 2. These machines are powered by a sinusoidal current. The machines' parameters and geometrical dimensions are listed in Table1.

Flux lines distribution in three studied machines is presented in Fig. 3. The effect of the three distinct values of soft-magnetic relative permeability (viz., 200, 800 and ∞) on the performances of the studied machines, are estimated analytically and compared by 2-D FEA. The *t*- and θ-component of the magnetic flux density waveform in the pitch circle of the air-gap (i.e., Subdomain VI) are calculated with a harmonic number of n = 100 at no-/on-load conditions in M1, M2 and M3 machines as presented in Figs. 4-6, respectively. The analytical estimation of magnetic flux distribution is done taking into account the same relative permeability in all iron parts. It is obvious that a good accordance is obtained for the *t*- and θ-components of the magnetic flux density.

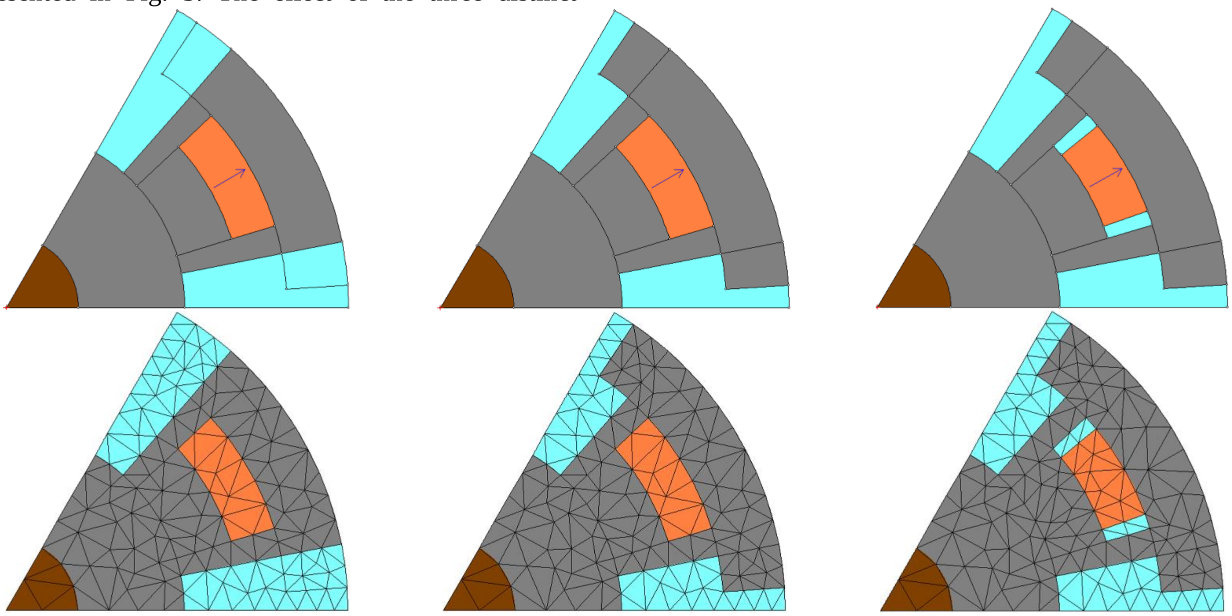

(a) (b) (c)

Fig. 2 The investigated IPM machines; a) M1, b) M2, and c) M3.

Table 1 The investigated IPM machines' parameters.

Symbol	Unit	Definition	Value M1 M2 M3
B_{rm}	T	Remanence flux density of PMs	1
μ_{rm}		PMs' relative permeability	1
N_c		Number of wires per slot	24
I_m	A	Phase current amplitude	10
Q_s		Stator slots number	18
c	deg.	Stator slot-opening	10
p		Number of pole pairs	3
R_4	mm	Radius of stator slots	82.75
R_3	mm	Radius of the stator inner surface	38.9
R_2	mm	Radius of the rotor outer surface at the PM surface	27.72
R_1	mm	Radius of the rotor inner surface at the PM bottom	15.92
g	mm	Air-gap length	1
L_u	mm	Axial length	80
n	rpm	Mechanical pulse of synchronism	8000
		Stator/rotor core material	M19-0.5mm

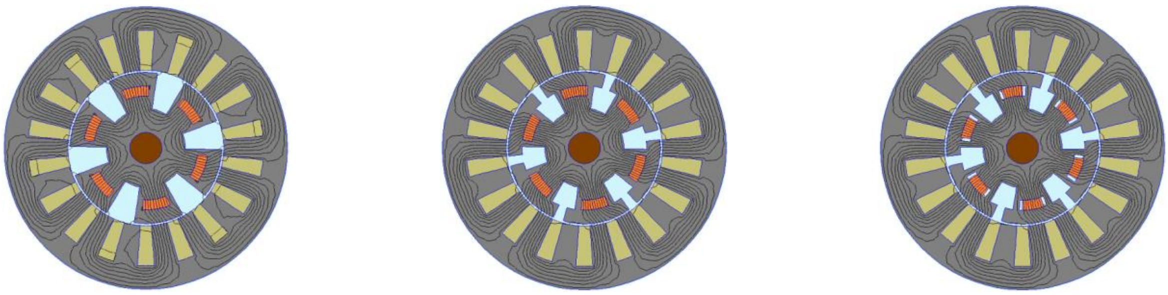

(a) (b) (c)

Fig. 3 Flux lines distribution in a) M1, b) M2, and c) M3 machines.

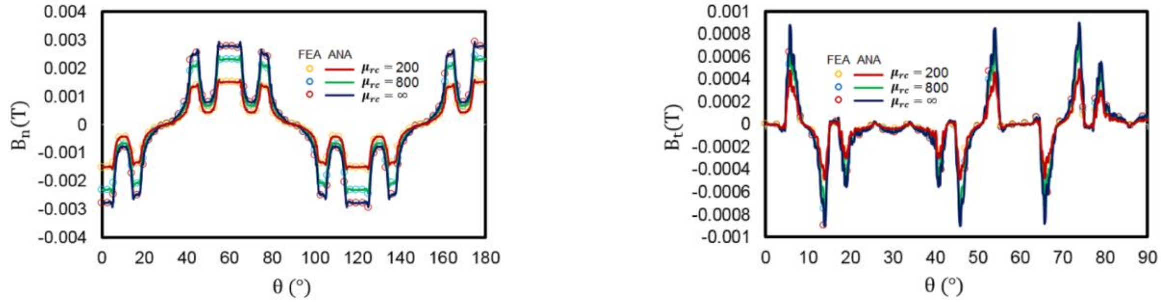

(a)

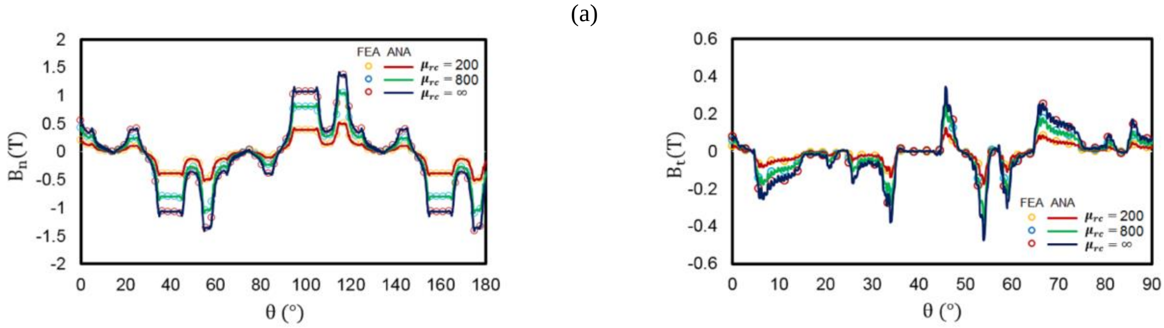

(b)

Fig. 4 The *t*- and θ- component of the magnetic flux density waveform in the pitch circle of the air-gap (i.e., Subdomain VI) at a) no-load, and b) on-load condition in M1 machine.

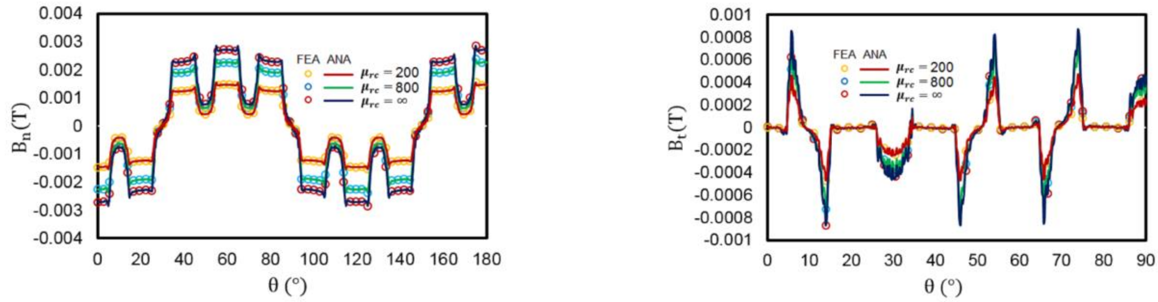

(a)

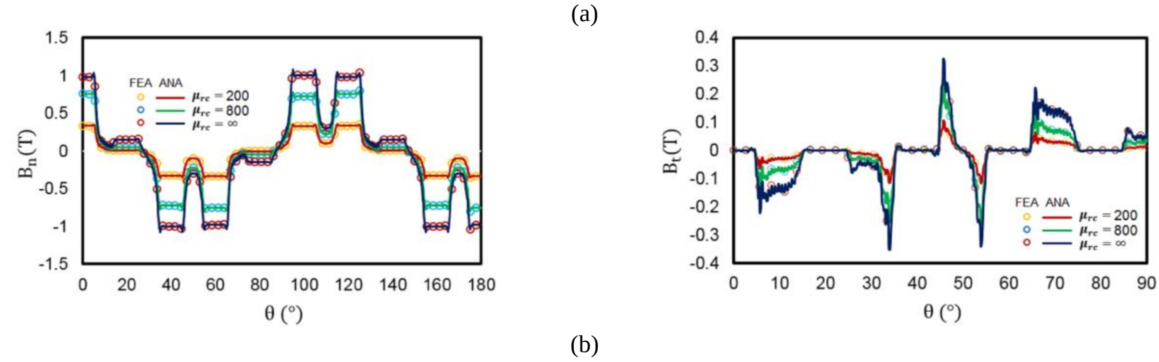

(b)

Fig. 5 The *t*- and θ- component of the the magnetic flux density waveform in the pitch circle of the air-gap (i.e., Subdomain VI) at a) no-load, and b) on-load condition in M2 machine.

The *x*- and *y*-components of the magnetic flux density waveform in the pitch circle of the air-gap (i.e., Subdomain VI) are calculated with a harmonic number of $n = 100$ at no-/on-load conditions in M1, M2 and M3 machines as shown in Figs. 7-9, respectively. It is obvious that a good accordance is obtained for the *t*- and *θ*-components of the magnetic flux density.

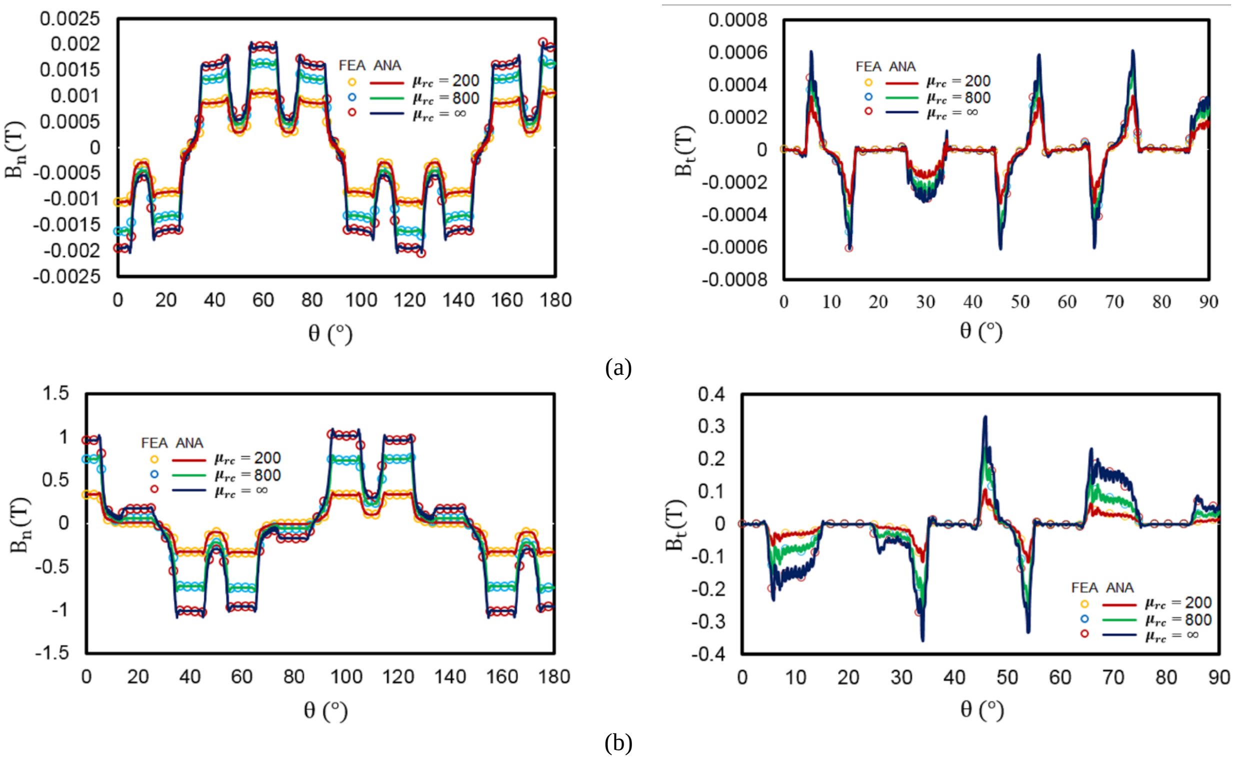

Fig. 6 The *t*- and *θ*- component of the the magnetic flux density waveform in the pitch circle of the air-gap (i.e., Subdomain VI) at a) no-load, and b) on-load condition in M3 machine.

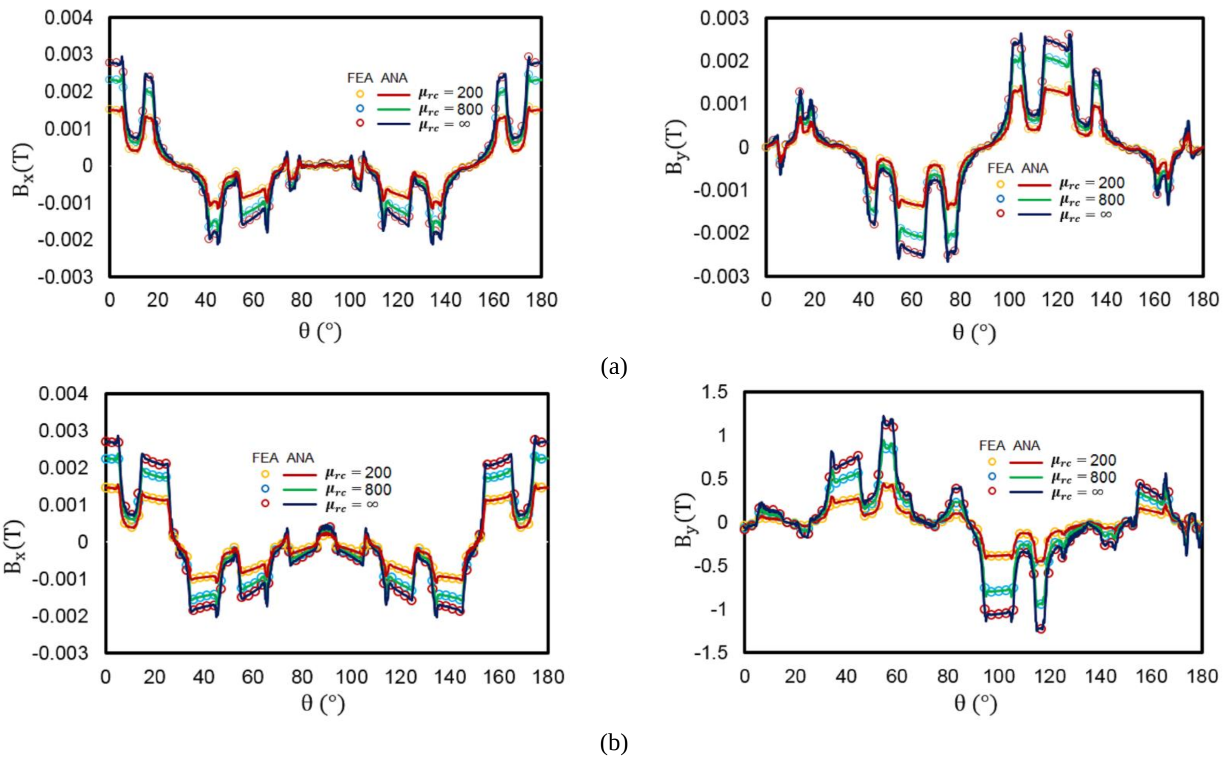

Fig. 7 The *x*- and *y*-component of the magnetic flux density waveform in the pitch circle of the air-gap at a) no-load, and b) on-load condition in M1 machine.

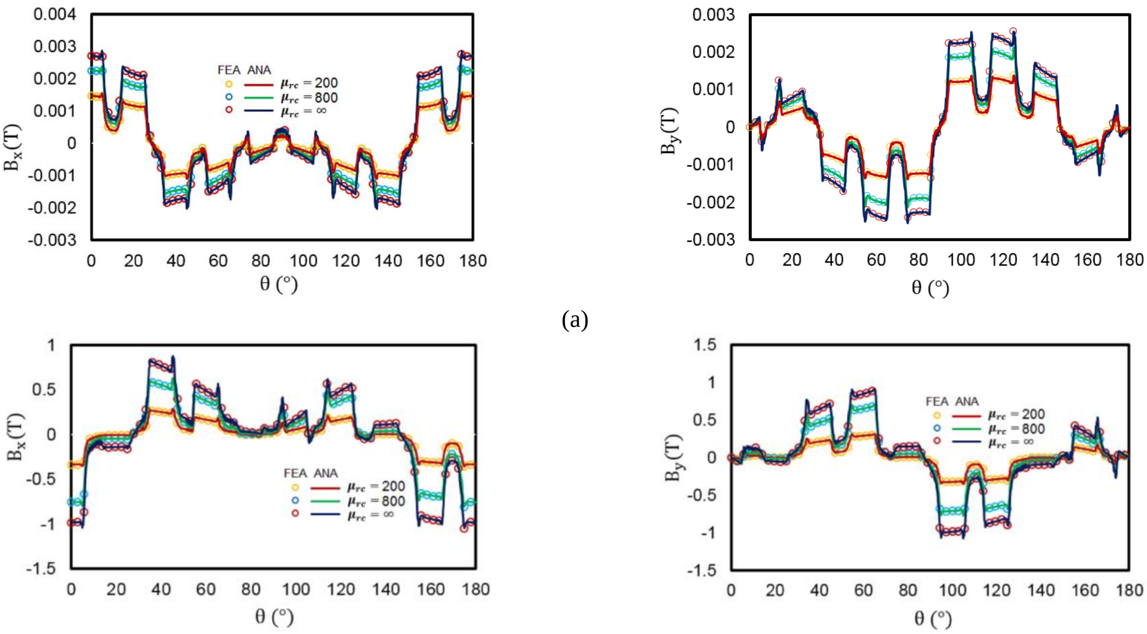

(a)

(b)

Fig. 8 The *x*- and *y*-component of the magnetic flux density waveform in the pitch circle of the air-gap at a) no-load, and b) on-load condition in M2 machine.

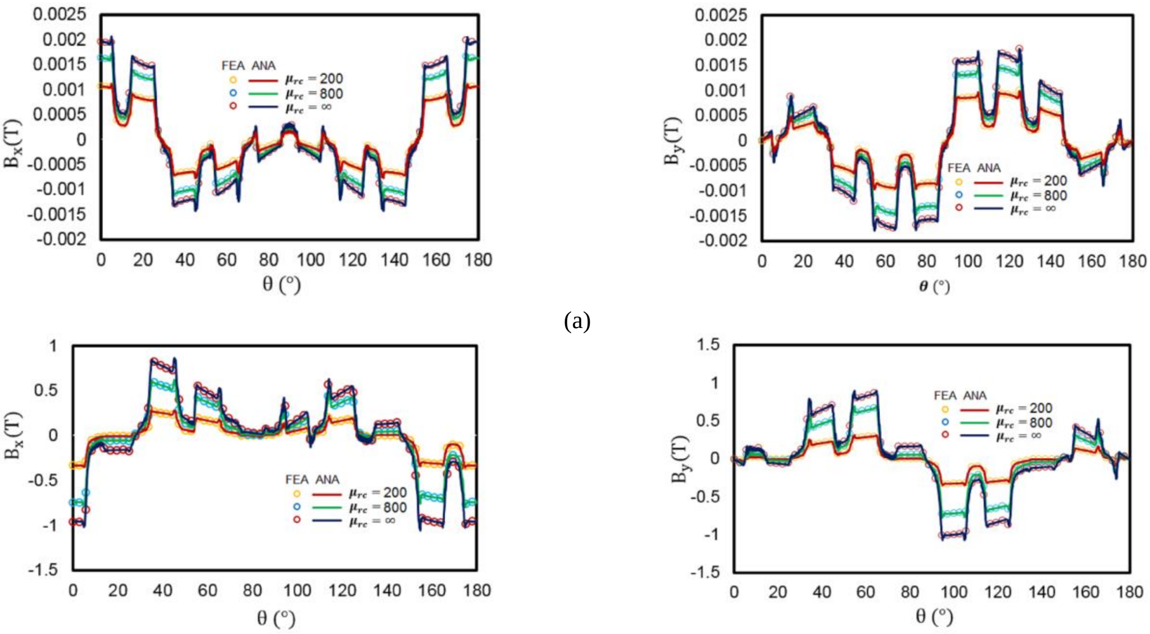

(a)

(b)

Fig. 9 The *x*- and *y*-component of the magnetic flux density waveform in the pitch circle of the air-gap at a) no-load, and b) on-load condition in M3 machine.

The *x*- and *y*-components of Maxwell tensor force waveform in the pitch circle of the air-gap at no-/on-load conditions in M1, M2, and M3 machines are computed analytically and compared to those obtained by numerical method for three different soft-magnetic material permeability as presented in Figs. 10-12, respectively. It is obvious that a good accordance is obtained for the *x*- and *y*-components of the Maxwell tensor force.

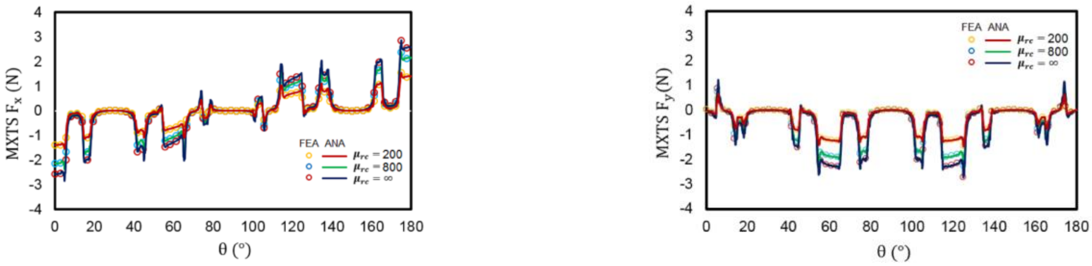

(a)

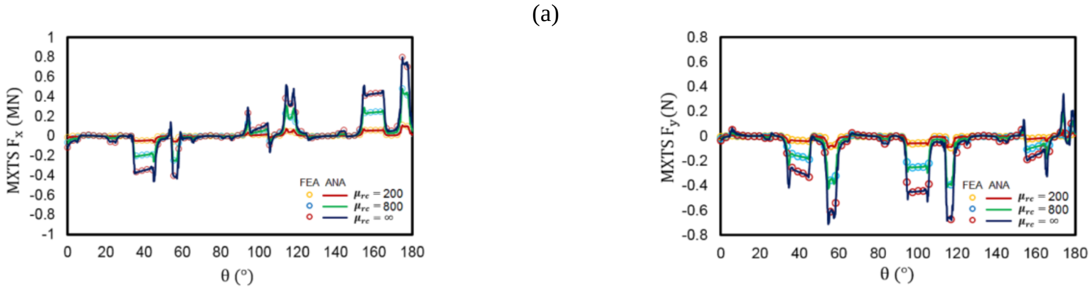

(b)

Fig. 10 The *x*- and *y*-component of Maxwell tensor force waveform in the pitch circle of the air-gap at a) no-load, and b) on-load condition in M1 machine.

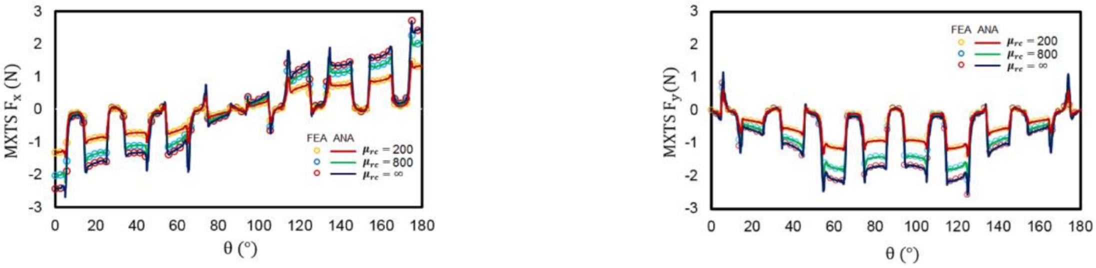

(a)

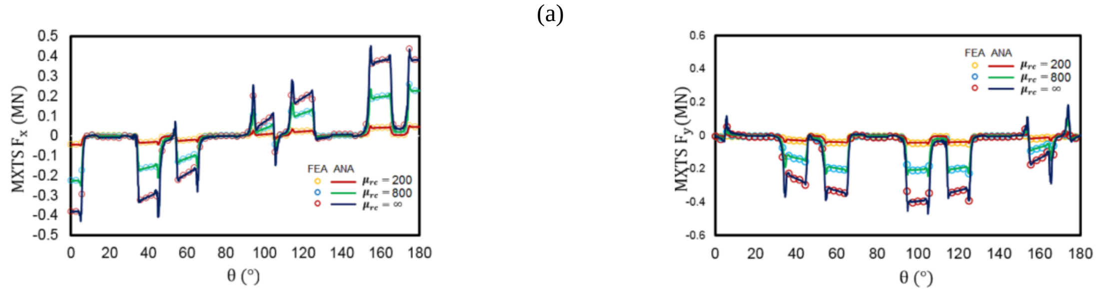

(b)

Fig. 11 The *x*- and *y*-component of Maxwell tensor force waveform in the pitch circle of the air-gap at a) no-load, and b) on-load condition in M2 machine.

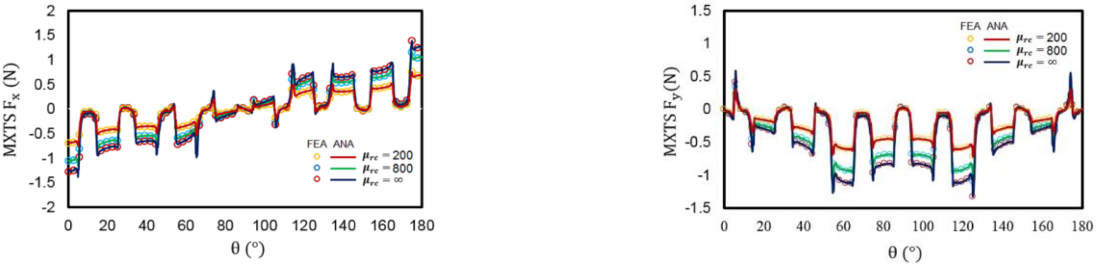

(a)

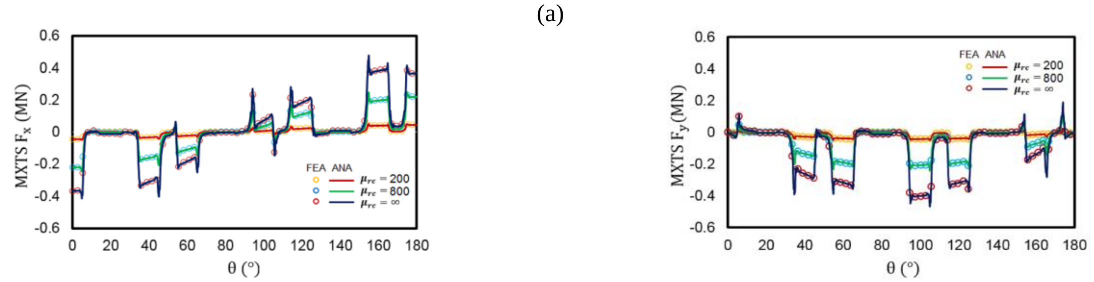

(b)

Fig. 12 The *x*- and *y*-component of Maxwell tensor force waveform in the pitch circle of the air-gap at a) no-load, and b) on-load condition in M3 machine.

A waveform comparison of the normal component of Maxwell tensor force in the pitch circle of the air-gap at no-/on-load conditions in M1, M2 and M3 machines are computed analytically and compared to those obtained by numerical method for three different soft-magnetic material permeability as presented in Figs. 13-15, respectively. The obtained results are in close accordance with the results of FEA.

A waveform comparison of Maxwell tensor torque in the pitch circle of the air-gap at no-/on-load conditions in M1, M2 and M3 machines are computed analytically and compared to those obtained by numerical method for three different soft-magnetic material permeability as presented in Figs. 16-18, respectively. The obtained results are in close accordance with the results of FEA.

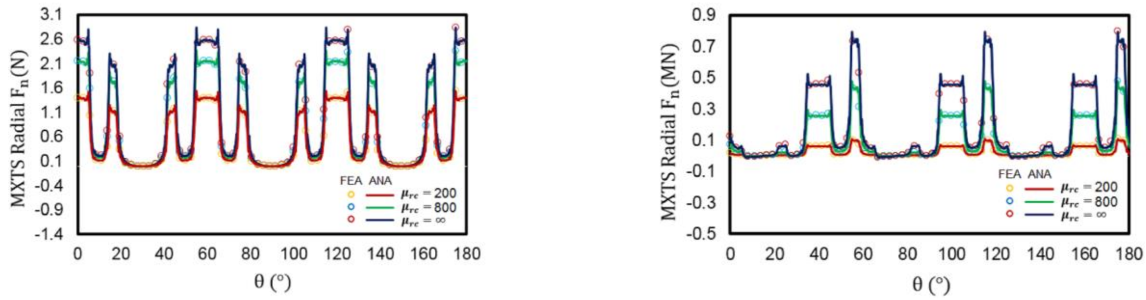

(a) (b)

Fig. 13 The normal component of Maxwell tensor force waveform in the pitch circle of the air-gap at a) no-load, and b) on-load condition in M1 machine.

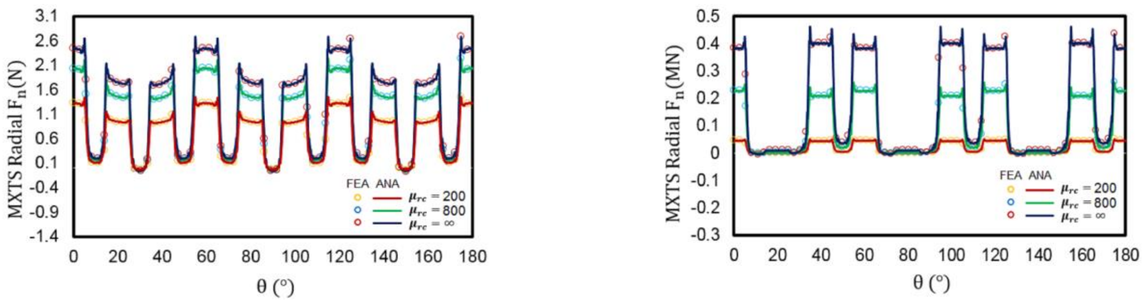

(a) (b)

Fig. 14 The normal component of Maxwell tensor force waveform in the pitch circle of the air-gap at a) no-load, and b) on-load condition in M2 machine.

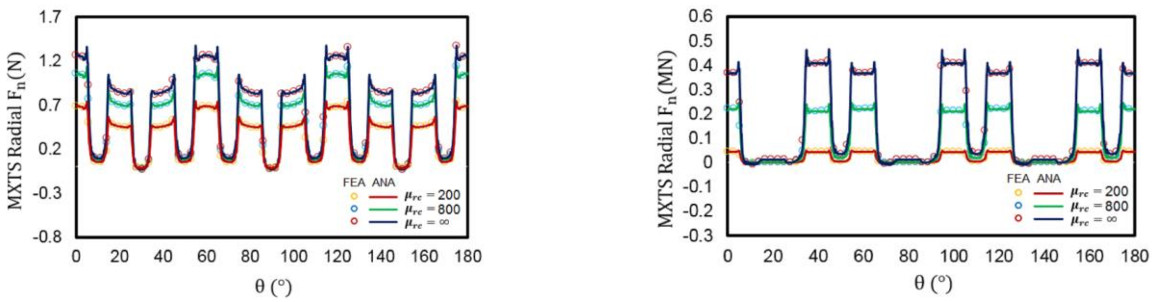

(a) (b)

Fig. 15 The normal component of Maxwell tensor force waveform in the pitch circle of the air-gap at a) no-load, and b) on-load condition in M3 machine.

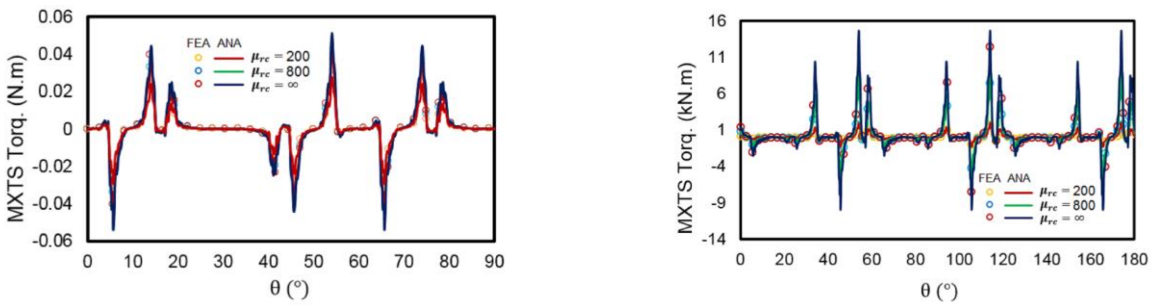

(a) (b)

Fig. 16 Maxwell tensor torque waveform in the pitch circle of the air-gap at a) no-load, and b) on-load condition in M1 machine.

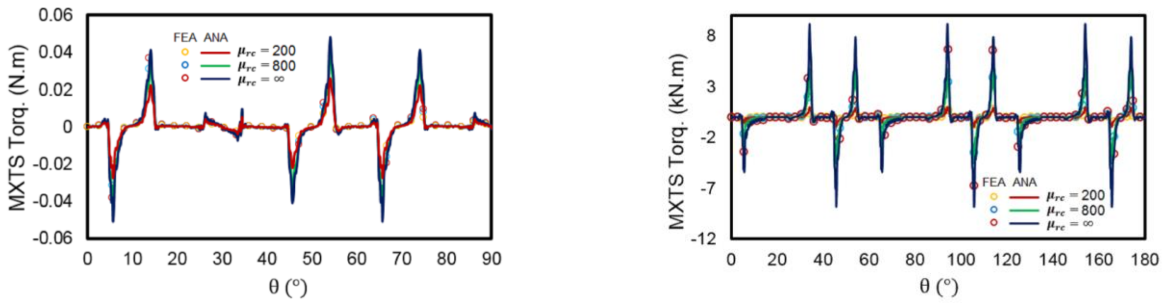

(a) (b)

Fig. 17 Maxwell tensor torque waveform in the pitch circle of the air-gap at a) no-load, and b) on-load condition in M2 machine.

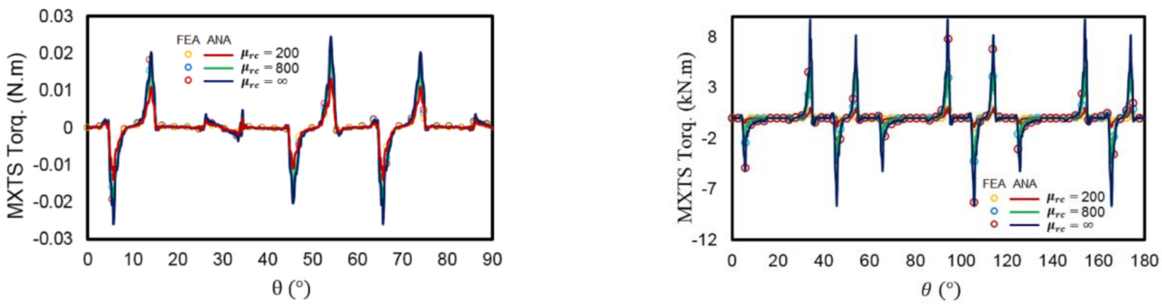

(a) (b)

Fig. 18 Maxwell tensor torque waveform in the pitch circle of the air-gap at a) no-load, and b) on-load condition in M3 machine.

7 Conclusions

A subdomain based semi-analytical model was presented in a pseudo-Cartesian coordinates system for the prediction of the no-/on-load electromagnetic performances in one magnet per pole IPM machines considering the distinct value of relative permeability in periodic/non-periodic subdomains. The general solution of Maxwell's equations in each periodic/non-periodic region has then been derived by using the principle of superposition. Appropriate BCs at the interface among the different subdomains were defined in two axis (i.e., t- and θ–edges), to compute the integration constants. It is clear that the results of the proposed model are in close accordance with those realized by 2-D FEA.

Acknowledgment

This research is carried out based on a research project which has been financially supported by the office of vice chancellor for research of Arak University with contract number of 98/1671.

References

[1] P. La Delfa, M. Hecquet, F. Gillon, and J. Le Besnerais, "Analysis of radial force harmonics in PMSM responsible for electromagnetic noise," in *Tenth International Conference on Ecological Vehicles and Renewable Energies (EVER)*, pp. 1–6, Mar. 2015.

[2] S. Jia, R. Qu, J. Li, Z. Fu, H. Chen, and L. Wu, "Analysis of FSCW SPM servo motor with static, dynamic and mixed eccentricity in aspects of radial force and vibration," in *IEEE Energy Conversion Congress and Exposition (ECCE)*, pp. 1745–1753, Sep. 2014.

[3] D. Y. Kim, J. K. Nam, and G. H. Jang, "Reduction of magnetically induced vibration of a spoke-type IPM motor using magnetomechanical coupled analysis and optimization," *IEEE Transactions on Magnetics*, Vol. 42, No. 9, pp. 5097–105, 2013.

[4] K. Boughrara, R. Ibtiouen, and F. Dubas, "Analytical prediction of electromagnetic performances and unbalanced magnetic forces in fractional-slot spoke-type permanent-magnet machines," in *XXII International Conference on Electrical Machines (ICEM)*, pp. 1366–1372, Sep. 2016.

[5] L. Roubache, M. B. Yahia, K. Boughrara, F. Dubas, and R. Ibtiouen, "Analytical modeling of electromagnetic noise in spoke-type permanent-magnet machines," in *International Conference on Electrical Sciences and Technologies in Maghreb (CISTEM)*, pp. 1–5, Oct. 2018.

[6] R. L. Sprangers, J. J. Paulides, B. L. Gysen, and E. A. Lomonova, "Magnetic saturation in semi-analytical harmonic modeling for electric machine analysis," *IEEE Transactions on Magnetics*, Vol. 52, No. 2, pp. 1–10, 2016.

[7] R. L. Sprangers, J. J. Paulides, B. L. Gysen, and E. A. Lomonova, "Semianalytical framework for synchronous reluctance motor analysis including finite soft-magnetic material permeability," *IEEE Transactions on Magnetics*, Vol. 51, No. 11, pp. 1–4, 2015.

[8] Z. Djelloul-Khedda, K. Boughrara, R. Ibtiouen, and F. Dubas, "Nonlinear analytical calculation of magnetic field and torque of switched reluctance machines," in *International Conference on Electrical Sciences and Technologies in Maghreb (CISTEM)*, pp. 1–8, Oct. 2016.

[9] Z. Djelloul-Khedda, K. Boughrara, F. Dubas, and R. Ibtiouen, "Nonlinear analytical prediction of magnetic field and electromagnetic performances in switched reluctance machines," *IEEE Transactions on Magnetics*, Vol. 53, No. 7, pp. 1–11, 2017.

[10] Z. Djelloul-Khedda, K. Boughrara, F. Dubas, A. Kechroud, and B. Souleyman, "Semi-analytical magnetic field predicting in many structures of permanent-magnet synchronous machines considering the iron permeability," *IEEE Transactions on Magnetics*, Vol. 54, No. 7, pp. 1–21, 2018.

[11] Z. Djelloul-Khedda, K. Boughrara, F. Dubas, A. Kechroud, and A. Tikellaline, "Analytical prediction of iron-core losses in flux-modulated permanent-magnet synchronous machines," *IEEE Transactions on Magnetics*, Vol. 55, No. 1, pp. 1–12, 2019.

[12] L. Roubache, K. Boughrara, F. Dubas and R. Ibtiouen, "Semi-analytical modeling of spoke-type permanent-magnet machines considering the iron core relative permeability: Subdomain technique and Taylor polynomial," *Progress In Electromagnetics Research*, pp. 85–101, 2017.

[13] F. Dubas and K. Boughrara, "New scientific contribution on the 2-D subdomain technique in Cartesian coordinates: taking into account of iron parts," *Mathematical and Computational Applications*, Vol. 22, No. 1, p. 17, 2017.

[14] F. Dubas and K. Boughrara, "New scientific contribution on the 2-D subdomain technique in polar coordinates: Taking into account of iron parts," *Mathematical and Computational Applications*, Vol. 22, No. 4, p. 42, 2017.

[15] L. Roubache, K. Boughrara, F. Dubas, and R. Ibtiouen, "New subdomain technique for electromagnetic performances calculation in radial-flux electrical machines considering finite soft-magnetic material permeability," *IEEE Transactions on Magnetics*, Vol. 54, No. 4, pp. 1–5, 2018.

[16] M. Ben Yahia, K. Boughrara, F. Dubas, L. Roubache, and R. Ibtiouen, "Two-dimensional exact subdomain technique of switched reluctance machines with sinusoidal current excitation," *Mathematical and Computational Applications*, Vol. 23, No. 4, pp. 59, 2018.

[17] L. Roubache, K. Boughrara, F. Dubas, and R. Ibtiouen, "Elementary subdomain technique for magnetic field calculation in rotating electrical machines with local saturation effect," *COMPEL-The International Journal for Computation and Mathematics in Electrical and Electronic Engineering*, Vol. 38, No. 1, pp. 24–45, 2019.

[18] M. Huo, S. Wang, J. Xiu, and S. Cao, "Effect of magnet/slot combination on triple-frequency magnetic force and vibration of permanent magnet motors," *Journal of Sound and Vibration*, Vol. 332, No. 22, pp. 5965–80, 2013.

[19] Y. S. Chen, Z. Q. Zhu, and D. Howe, "Vibration of PM brushless machines having a fractional number of slots per pole," *IEEE Transactions on Magnetics*, Vol. 42, No. 10, pp. 3395–3397, 2006.

[20] A. Jabbari, M. Shakeri, and S. A. Nabavi Niaki, "Pole shape optimization of permanent magnet synchronous motors using the reduced basis technique," *Iranian Journal of Electrical and Electronic Engineering*, Vol. 6, No. 1, pp. 48-55, 2010.

[21] A. Jabbari, "2D analytical modeling of magnetic vector potential in surface mounted and surface inset permanent magnet machines," *Iranian Journal of Electrical and Electronic Engineering*, Vol. 13, No. 4, pp. 362–373, 2017.

[22] A. Jabbari, "Exact analytical modeling of magnetic vector potential in surface inset permanent magnet DC machines considering magnet segmentation," *Journal of Electrical Engineering*, Vol. 69, No. 1, pp. 39–45, 2018.

[23] A. Jabbari, "An analytical expression for magnet shape optimization in surface-mounted permanent magnet machines," *Mathematical and Computational Applications*, Vol. 23, No. 4, p. 57, 2018.

[24] A. Jabbari, "Analytical modeling of magnetic field distribution in multiphase H-type stator core permanent magnet flux switching machines," *Iranian Journal of Science and Technology, Transactions of Electrical Engineering*, pp. 1–3, 2018.

[25] A. Jabbari, "An analytical expression for magnet shape optimization in surface-mounted permanent magnet machines," *Mathematical and Computational Applications*, Vol. 23, No. 4, pp. 57, 2018.

[26] A. Jabbari and F. Dubas, "Analytical modeling of magnetic field distribution in spoke type permanent magnet machines," *Journal of Iranian Association of Electrical and Electronics Engineers*, Accepted.

[27] F. Dubas and C. Espanet, "Analytical solution of the magnetic field in permanent-magnet motors taking into account slotting effect: No-load vector potential and flux density calculation," *IEEE Transactions on Magnetics*, Vol. 45, No. 5, pp. 2097–2109, 2009.

[28] E. Devillers, J. Le Besnerais, T. Lubin, M. Hecquet, and J. P. Lecointe, "A review of subdomain modeling techniques in electrical machines: performances and applications," in *XXII International Conference on Electrical Machines (ICEM)*, pp. 86–92, Sep 2016.

[29] H. Tiegna, Y. Amara, and G. Barakat, "Overview of analytical models of permanent magnet electrical machines for analysis and design purposes," *Mathematics and Computers in Simulation*, Vol. 90, pp. 162–77, 2013.

[30] M. Curti, J. J. Paulides, and E. A. Lomonova, "An overview of analytical methods for magnetic field computation," in *Tenth International Conference on Ecological Vehicles and Renewable Energies (EVER)*, pp. 1–7, Mar. 2015.

[31] P. D. Pfister, X. Yin, and Y. Fang, "Slotted permanent-magnet machines: General analytical model of magnetic fields, torque, eddy currents, and permanent-magnet power losses including the diffusion effect," *IEEE Transactions on Magnetics*, Vol. 52, No. 5, pp. 1–3.

[32] F. Dubas and A. Rahideh, "Two-dimensional analytical permanent-magnet eddy-current loss calculations in slotless PMSM equipped with surface-inset magnets," *IEEE Transactions on Magnetics*, Vol. 50, No. 3, pp. 54–73, 2014.

[33] K. Boughrara, R. Ibtiouen, and T. Lubin, "Analytical prediction of magnetic field in parallel double excitation and spoke-type permanent-magnet machines accounting for tooth-tips and shape of polar pieces," *IEEE Transactions on Magnetics*, Vol. 48, No. 7, pp. 2121–2137, 2012.

[34] T. Lubin, S. Mezani, and A. Rezzoug, "Two-dimensional analytical calculation of magnetic field and electromagnetic torque for surface-inset permanent-magnet motors," *IEEE Transactions on Magnetics*, Vol. 48, No. 6, pp. 2080–2091, 2012.

[35] P. Liang, F. Chai, Y. Li, and Y. Pei, "Analytical prediction of magnetic field distribution in spoke-type permanent-magnet synchronous machines accounting for bridge saturation and magnet shape," *IEEE Transactions on Industrial Electronics*, Vol. 64, No. 5, pp. 3479–3488, 2017.

[36] M. Pourahmadi-Nakhli, A. Rahideh and M. Mardaneh, "Analytical 2-D model of slotted brushless machines with cubic spoke-type permanent magnets," *IEEE Transactions on Energy Conversion*, Vol. 33, No. 1, pp. 373–382, 2018.

[37] K. Boughrara, N. Takorabet, R. Ibtiouen, O. Touhami, and F. Dubas, "Analytical analysis of cage rotor induction motors in healthy, defective, and broken bars conditions," *IEEE Transactions on Magnetics*, Vol. 51, No. 2, pp. 1–7, 2015.

[38] L. Roubache, K. Boughrara, and R. Ibtiouen, "Analytical electromagnetic analysis of multi-phases cage rotor induction motors in healthy, broken bars and open phases conditions," *Progress In Electromagnetics Research*, Vol. 70, pp. 113–130, 2016.

[39] K. Boughrara, F. Dubas, and R. Ibtiouen, "2-D analytical prediction of eddy currents, circuit model parameters, and steady-state performances in solid rotor induction motors," *IEEE Transactions on Magnetics*, Vol. 50, No. 12, pp. 1–4, 2014.

A. Jabbari was born in Shazand, Iran, in 1980. He received the B.Sc. degree from the Iran University of Science and Technology in 2002 and his M.Sc. and Ph.D. degrees both in Mechanical Engineering from the Mazandran University, in 2004 and 2009, respectively, with a focus on the design and the optimization of Brushless DC permanent magnet machines for direct drive applications. He is currently an Assistant Professor with the Department of Mechanical Engineering, Arak University, Arak, Iran. Since 2014, he has been the Head of Gearless Wind Turbine Project team.
Interests: gearless wind turbine design, analytical modeling, PM machines, subdomain technique, friction stir welding, metal forming.

F. DUBAS was born in Vesoul, France, in 1978. He received the M.Sc. degree from the Université of Franche-Comté" (UFC) in 2002 and the Ph.D. degree from the UFC in 2006, with a focus on the design and the optimization of high-speed surface-mounted permanent-magnet (PM) synchronous motor for the drive of a fuel cell air-compressor. He is currently an Associate Professor with the Département ENERGIE, FEMTO-ST Institute affiliated to the CNRS and jointly with the University Bourgogne Franche-Comté. In 2014 to 2016, he has been the Head of Unconventional Thermal and Electrical

Machines Team. He is the Head of the "Electrical Actuators" group in the Hybrid & Fuel Cell Systems, Electrical Machines (SHARPAC) Team. He works with ALSTOM Transports (France), and RENAULT (France), where he is involved in the modeling, design, and optimization of electrical systems and, in particular, induction and PM synchronous (radial and/or axial flux) machines, creative problem solving, and electrical propulsion/traction. He has authored over 100 refereed publications and he holds a patent about the manufacturing of axial-flux PM machines with flux-focusing. Dr. Dubas received the Prize Paper Awards in the IEEE Conference Vehicle Power and Propulsion (VPPC) in 2005 as well as the Prize Presentation Awards in the 19th International Conference on Electrical Machines and Systems (ICEMS) in 2017.
Interests: applied mathematics; partial differential equations, separation of variables method; principle of superposition; (semi-)analytical modeling; subdomain technique; magnetic equivalent circuit; electrical machines.